

Potential energy surfaces inference of both ground and excited state using hybrid quantum-classical neural network

Yasutaka Nishida and Fumihiko Aiga

Corporate Research & Development Center, Toshiba Corporation, 1 Komukai-Toshiba-cho, Saiwai-ku, Kawasaki 212-8582, Japan

Reflecting the increasing interest in quantum computing, the variational quantum eigensolver (VQE) has attracted much attentions as a possible application of near-term quantum computers. Although the VQE has often been applied to quantum chemistry, high computational cost is required for reliable results because infinitely many measurements are needed to obtain an accurate expectation value and the expectation value is calculated many times to minimize a cost function in the variational optimization procedure. Therefore, it is necessary to reduce the computational cost of the VQE for a practical task such as estimating the potential energy surfaces (PESs) with chemical accuracy, which is of particular importance for the analysis of molecular structures and chemical reaction dynamics. A hybrid quantum-classical neural network has recently been proposed for surrogate modeling of the VQE [Xia *et al*, *Entropy* **22**, 828 (2020)]. Using the model, the ground state energies of a simple molecule such as H₂ can be inferred accurately without the variational optimization procedure. In this study, we have extended the model by using the subspace-search variational quantum eigensolver procedure so that the PESs of the both ground and excited state can be inferred with chemical accuracy. We also demonstrate the effects of sampling noise on performance of the pre-trained model by using IBM's QASM backend.

1 Introduction

Together with recent advances in quantum hardware, the application field of quantum computation has expanded to encompass physics [1, 2, 3], chemistry [4, 5, 6], machine learning [7, 8, 9, 10, 11, 12], biology [13], and finance [14]. Although promising applications of quantum computation for industry are still at the theoretical stage, the possibility of quantum advantage or required resource estimation for such applications is being actively studied [15, 16, 17, 18]. Quantum computers currently under development are called noisy intermediate-scale quantum (NISQ) [19] devices. An NISQ has high noise level and can only perform imperfect operations with a limited coherence time. Therefore, many hybrid quantum-classical algorithms [20, 21, 22, 23] have been developed to find an efficient use of this limited quantum resources.

The variational quantum eigensolver (VQE) [20, 21] is one of the hybrid quantum-classical algorithms for solving electronic structure problems on quantum hardware. The

Yasutaka Nishida: yasutaka.nishida@toshiba.co.jp

VQE is a quantum heuristic algorithm, where a target expectation value is calculated based on the outcome from measurement on quantum hardware and parameters of a quantum circuit are updated to minimize the expectation value on a classical computer. This variational optimization procedure is performed by iterating a closed feedback loop between classical and quantum hardware. To obtain accurate expectation values in the VQE procedure, a number of measurements and the averaging of their results are required [24]. Therefore, for practical use, reduction techniques [25] for qubit and measurement [26, 27] have been actively studied. Furthermore, to extract a correct average value from noisy output or shorten computational runtimes, error mitigation techniques [28] and efficient optimization methods [29, 30] have been studied.

As regards other approaches for the practical use of quantum algorithms on NISQ devices, quantum machine learning has also been introduced [12, 31, 32, 33]. One such approach is applied to surrogate modeling or to building a generalized model to output VQE results in the field of quantum chemistry. For example, a Hamiltonian-alternating ansatz using a few training data points [31] or a hybrid quantum-classical neural network (HQCNN) model [32, 33] are proposed. Since these generalized quantum circuits make it possible to infer the ground state energies accurately at any chemical configuration without the variational optimization procedure, calculation runtimes of PESs can be reduced drastically.

In this paper, we have developed an HQCNN to estimate PESs of both ground and excited state, where the subspace-search variational quantum eigensolver (SSVQE) [34] is used for minimizing a cost function. Our model is an extended model of the HQCNN proposed by Xia [32]. A schematic approach is illustrated in Fig. 1. The difference between our work and Xia’s is that we prepare mutually orthogonal initial states for calculating a cost function, and then the cost function is defined as a weighted sum of their energies. We apply our model to the H_2 molecule and find that the pre-trained model can estimate PESs of both the ground and excited state with high accuracy. We also investigate the effects of sampling noise on performance of the pre-trained model by using IBM’s QASM backend [44], where our model is trained by a noiseless simulator and then PESs are inferred using the pre-trained model on IBM’s qasm simulator. As a result, the relative errors between results from our model and the exact solution satisfy the chemical accuracy at 10^5 QASM shots.

The paper is organized as follows. In Sec. 2, we briefly explain the procedure of VQE, SSVQE, and our HQCNN model. This is followed by the details of our implementation. In Sec. 3, we present our results and analyses that follow from our data. In Sec. 4, we discuss our results and outline open perspectives, and summarize in Sec. 5.

2 Methods

A surrogate model we have developed is explained in detail. Before proceeding to our model, we briefly review the VQE and the SSVQE.

2.1 Variational quantum eigensolver

The variational quantum eigensolver (VQE) [20, 21] is a variational algorithm that relies upon the Rayleigh-Ritz variational principle of quantum mechanics. A variational optimization procedure of the VQE minimizes the expectation value of a Hamiltonian by iterating a closed feedback loop between classical and quantum hardware. When a molecular Hamiltonian is given, the VQE can find its ground state energy and the ground state

is generated on quantum hardware by an optimized parameterized quantum circuit, where the Hamiltonian is transformed into qubit representation from its second quantization representation. For an n -qubits system, a molecular Hamiltonian can be written as the sum of tensor products of Pauli matrices,

$$\mathcal{H} = \sum_{P \in \{I, X, Y, Z\}^{\otimes n}} h_P P, \quad (1)$$

where I, X, Y, Z are single-qubit Pauli operators and $h_p \in \mathbb{R}$ is a coefficient. The transformation of Eq. (1) is done by the Jordan–Wigner transformation [35, 36], the Bravyi–Kitaev transformation [37, 38] or other methods [35, 37, 39]. The expectation value of the qubit Hamiltonian is evaluated on a classical computer by summing each expectation value of P for $h_p \neq 0$ term which is the outcome from measurement on quantum hardware. To generate an initial quantum state in the VQE procedure, an initialized state $|0\rangle := |0\rangle^{\otimes n}$ is fed into a parameterized quantum circuit $U(\vec{\theta})$. The classical parameters $\vec{\theta}$ of U are updated to minimize the energy expectation value of $E(\vec{\theta}) = \langle 0|U^\dagger(\vec{\theta})\mathcal{H}U(\vec{\theta})|0\rangle$, where the updated parameters are fed back into the parameterized quantum circuit until $E(\vec{\theta})$ converges. When the minimal energy is reached, the optimal parameter $\vec{\theta}^*$ is determined. The VQE algorithm can be summarized as follows:

- (i) Define a quantum circuit $U(\vec{\theta})$ with parameters $\vec{\theta}$.
- (ii) Repeat the following procedures until $E(\vec{\theta})$ converges.
 - (a) Generate a quantum state $|\psi(\vec{\theta})\rangle = U(\vec{\theta})|0\rangle$.
 - (b) Evaluate the energy $E(\vec{\theta})$ by measuring $\langle 0|U^\dagger(\vec{\theta})\mathcal{H}U(\vec{\theta})|0\rangle$.
 - (c) Update the parameters $\vec{\theta}$ to minimize $E(\vec{\theta})$.

When the convergence is reached, $E(\vec{\theta})$ is expected to be an approximate ground state energy.

2.2 Subspace-search variational quantum eigensolver

The subspace-search variational quantum eigensolver (SSVQE) [34] is an extended algorithm of the VQE. The SSVQE utilizes the conservation of orthogonality under the unitary transformation. To search low-energy subspace of a given Hamiltonian, mutually orthogonal initial states are prepared and fed into a parameterized quantum circuit. The variational optimization is performed by minimizing a cost function defined as a weighted sum of energies of the mutually orthogonal quantum states. The procedure of the SSVQE algorithm can be summarized as follows.

- (i) Define a quantum circuit $U(\vec{\theta})$ and mutually orthogonal initial states (reference states) $\{|\phi_j\rangle\}_{j=0}^{k-1}$ where $\langle \phi_i|\phi_j\rangle = \delta_{ij}$ is satisfied. For a 4-qubit case, the computational basis $\{|0000\rangle, |0001\rangle\}$ can be chosen as the two orthogonal reference states.
- (ii) Repeat the following steps until a cost function is minimized.
 - (a) Generate mutually orthogonal quantum states $|\psi_j(\vec{\theta})\rangle = U(\vec{\theta})|\phi_j\rangle$.
 - (b) Evaluate a cost function defined as a weighted sum of energies of mutually orthogonal quantum states $|\psi_j(\vec{\theta})\rangle$, $L_\omega(\vec{\theta}) = \sum_{j=0}^{k-1} \omega_j \langle \psi_j(\vec{\theta})|\mathcal{H}|\psi_j(\vec{\theta})\rangle$, where the vector of weight $\{\omega_j\}$ is chosen such that $\omega_0 > \omega_1 > \dots > \omega_{k-1} > 0$.
 - (c) Update the parameters $\vec{\theta}$ to minimize L_ω .

The vector of weight $\{\omega_j\}$ has the effect of adjusting which $|\phi_j\rangle$ converges to which excited state. When the cost function $L_\omega(\vec{\theta})$ converges, $U(\vec{\theta})$ maps the reference state $|\phi_j\rangle$ to the j th excited state $|\psi_j(\vec{\theta})\rangle$ of a given Hamiltonian.

2.3 Surrogate model of SSVQE

A surrogate model aims to generalize the outputs from a particular operation and reduce its computational cost. In the previous study [32], a hybrid quantum-classical neural network (HQCNN) is proposed to generalize outputs from a circuit optimized by the VQE. The HQCNN model can be regarded as a combining network between linear operations of quantum circuits and nonlinear operations of measurements and can infer the PES of the ground state with high accuracy for simple molecules such as H₂, LiH, and BeH₂ [32]. In this study, we extend the original HQCNN model so that both the ground and excited state energies can be inferred at once. Our strategy is as follows. In the original model, a VQE-based procedure is used as unsupervised training for optimizing the quantum-classical neural network, where the energy summation of each input data point is minimized. In our model, the VQE-based training procedure is replaced with an SSVQE one. Fig. 1 shows our extended HQCNN model for two orthogonal reference states of $|\phi_0\rangle$ and $|\phi_1\rangle$.

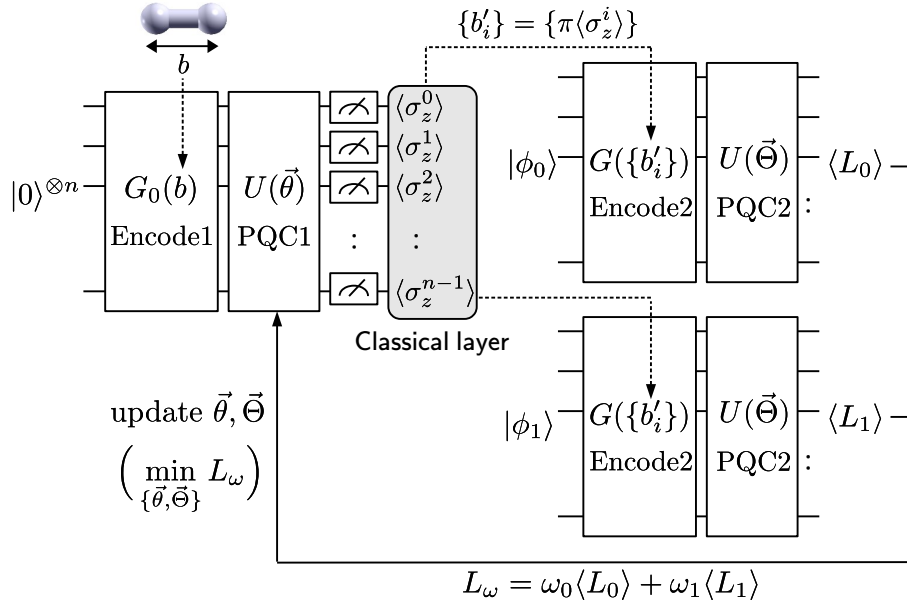


Figure 1: Our proposed extended quantum-classical hybrid neural network. Encode1 and Encode2 represent encode layers, and PQC1 and PQC2 represent parameterized quantum circuits U . In the first layer, bond length b is given as an input parameter of Encode1, G_0 , and then each qubit measurement is performed. The expectation value of Pauli-Z matrices $\langle \sigma_z^i \rangle$ calculated from i_{th} qubit measurement are fed into Encode2 as an input $\{b'_i\} = \{\pi \langle \sigma_z^i \rangle\}$ of G . $|\phi_0\rangle$ and $|\phi_1\rangle$ represent orthogonal reference states that finally converges to ground state and 1st excited state, respectively. $\langle L_0 \rangle$ and $\langle L_1 \rangle$ are the summation of the expectation value of each Hamiltonian calculated from training data points for each reference state $|\phi_0\rangle$ and $|\phi_1\rangle$, respectively. The parameters $\vec{\theta}$ and $\vec{\Theta}$ in PQC1 and PQC2 are optimized to minimize cost function $L_\omega = \omega_0 \langle L_0(\{\vec{\theta}, \vec{\Theta}\}) \rangle + \omega_1 \langle L_1(\{\vec{\theta}, \vec{\Theta}\}) \rangle$. Graphics of H₂ molecule is generated by XCrySDen [40].

The details of implementation can be summarized as follows.

2.3.1 Data encoding

The first step is to encode the input classical data into a quantum state. On the basis of the previous work [32], the encode gate G for an n -qubits system is generally defined as, $G = \otimes_{i=0}^{n-1} g_i(f_i(a_i))$ where g_i is a set of single qubit quantum gates on qubit i and f_i is a classical function to encode a_i as the parameter of g_i . The encode circuit G is initialized in the $|0\rangle^{\otimes n}$. An example of G is written as follows,

$$G(\{a_i\}) = \otimes_{i=0}^{n-1} R_y(a_i)H, \quad (2)$$

where R_y is the rotation- y gate and H is the Hadamard gate. In this work, we focus on a simple diatomic molecule, H_2 . Therefore, the bond length b is set as input data, so that the encode gate G_0 having one input parameter can be written as follows,

$$G_0(b) = \otimes_{i=0}^{n-1} R_y(b)H. \quad (3)$$

2.3.2 Parameterized Quantum Circuit

The second step is to build a parameterized quantum circuit (PQC) that consists of individual qubit rotations and qubit entangling parts. As all quantum gates used in a quantum circuit are unitary, a PQC itself is described as a unitary operation on n -qubits, $U(\vec{\theta})$. Since the expressibility and entangling capability of a PQC depend on its circuit structure [41], design of a circuit structure is important for inference performance of the HQCNN. Here, we use a simple circuit of RealAmplitudes comprising alternating R_y rotation gates on a single qubit and controlled-X (CX) gates. For the n -qubit case, the PQC with circuit depth $D(\geq 1)$ is expressed by

- n is even

$$U(\vec{\theta}) = \prod_{d=1}^D (\otimes_{i=0}^{n-1} R_y(\theta_{i+n(d-1)})) (CX_{n-3,n-2} \cdots CX_{1,2}) (CX_{n-2,n-1} \cdots CX_{0,1}), \quad (4)$$

- n is odd

$$U(\vec{\theta}) = \prod_{d=1}^D (\otimes_{i=0}^{n-1} R_y(\theta_{i+n(d-1)})) (CX_{n-2,n-1} \cdots CX_{1,2}) (CX_{n-3,n-2} \cdots CX_{0,1}), \quad (5)$$

where $CX_{m,n}$ represents CX gate with m as the control qubit and n is the target qubit. Examples of $U(\vec{\theta})$ in $n = 4$ and 5 cases are illustrated in Fig. 2. Here, the depth D is defined by the repetition number of the block circuit as shown in Fig. 2. For $U(\vec{\theta})$ with n -qubits and D depth, the number of the parameters is nD , $\vec{\theta} = \{\theta_0, \theta_1, \dots, \theta_{nD-1}\}$.

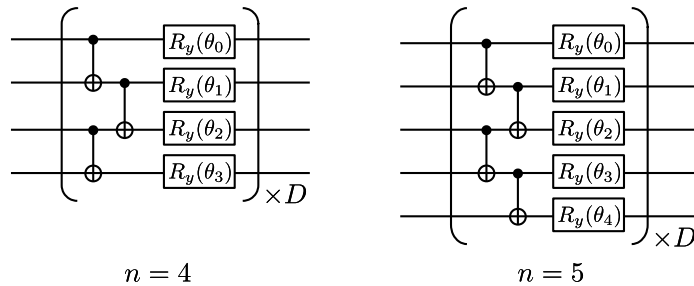


Figure 2: Examples of a PQC based on RealAmplitudes circuits with D depth in $n = 4, 5$ cases.

2.3.3 Classical layer

In Fig. 1, the measurement followed by PQC1 is a classical layer that corresponds to the activation function connecting between quantum layers. The classical layer measures the expectation value of Pauli-Z matrices of each qubit i , $\langle \sigma_z^i \rangle$. The values of $\langle \sigma_z^i \rangle$ are fed into the second encode layer as $G(\{\pi \langle \sigma_z^i \rangle\})$, and then the reference states $|\phi_j\rangle$ are encoded into a quantum state.

2.3.4 Cost function

A cost function is defined as a weighted energy summation of each reference state,

$$L_\omega(\vec{\theta}, \vec{\Theta}) = \sum_{j=0}^{k-1} \omega_j \langle L_j \rangle, \quad (6)$$

where $\langle L_j \rangle$ is the summation of the expectation value of each Hamiltonian calculated from training data points for each reference state $|\phi_j\rangle$. As explained in Sec. 2.2, the relation of $\omega_0 > \omega_1 > \dots > \omega_{k-1} > 0$ is satisfied. When the training points are chosen as $\vec{b} = \{b_0, b_1, \dots, b_{\alpha-1}\}$, $\langle L_j \rangle$ is calculated by

$$\langle L_j \rangle = \frac{1}{\alpha} \sum_{m=0}^{\alpha-1} \langle \psi_j(b_m) | U^\dagger(\vec{\Theta}) \mathcal{H}(b_m) U(\vec{\Theta}) | \psi_j(b_m) \rangle, \quad (7)$$

$$|\psi_j(b_m)\rangle = G(\{\pi \langle \sigma_{z,m}^i \rangle\}) |\phi_j\rangle, \quad (8)$$

$$\langle \sigma_{z,m}^i \rangle = \langle \psi(b_m) | U^\dagger(\vec{\theta}) (I \otimes I \cdots I \otimes \underbrace{Z}_{i\text{th}} \otimes I \cdots I \otimes I) U(\vec{\theta}) | \psi(b_m) \rangle, \quad (9)$$

$$|\psi(b_m)\rangle = G_0(b_m) |0\rangle. \quad (10)$$

For the n -qubits PQC with D depth, the cost function of Eq. (6) is a function of $2nD$ -dimensional vectors, i.e., $L_\omega(\{\theta_0, \theta_1, \dots, \theta_{nD-1}\}, \{\Theta_0, \Theta_1, \dots, \Theta_{nD-1}\})$. In the $k = 2$ case, the cost function is given by

$$L_\omega(\vec{\theta}, \vec{\Theta}) = \omega_0 \langle L_0 \rangle + \omega_1 \langle L_1 \rangle. \quad (11)$$

When the weight ω_j is fixed as $(\omega_0, \omega_1) = (1, 0)$, our model corresponds to Xia's original model [32] which can estimate only ground state energies. For estimating both energies of ground state and 1st excited state, we only have to set an appropriate weight such as $(\omega_0, \omega_1) = (1, 0.5)$ to satisfy $\omega_0 > \omega_1$. To check validity of our implementation, the trivial case of the $(\omega_0, \omega_1) = (1, 0)$ model is discussed in Sec. 3.

2.3.5 Optimization and computational conditions

The parameters $\vec{\theta}$ and $\vec{\Theta}$ of the PQC are updated to minimize the cost function L_ω . The optimization is performed by the Broyden–Fletcher–Goldfarb–Shanno algorithm [42] provided in the SciPy library [43]. The entire simulation of the quantum circuit is performed by Qiskit [44], where the statevector or backend noise model (QASM) simulator is available. The computational conditions are set as maximum iterations and gradient norm tolerance of 1000 and 10^{-5} , respectively. The qubit Hamiltonian of the equation (1) at each chemical configuration is transformed from its second quantization representation by OpenFermion [46], where the second quantization Hamiltonian is calculated by STO-3G minimal basis using PySCF [45]. The transformation of Eq. (1) is done by the Jordan–Wigner transformation [35, 36].

3 Numerical simulation and results

Using our HQCNN model, PES inference for the H_2 molecule is performed. In this simulation, each Hamiltonian of H_2 is transformed into 4-qubit Hamiltonian ($n = 4$) while varying its bond length. To train the PQC, a few training data points are used as $b_{\text{train}} = \{0.45, 0.85, 1.25, 1.65, 2.05, 2.45\}$ Å. The parameters of U are optimized on the statevector simulator in Qiskit [44], i.e., a noiseless simulator. Other computational conditions are summarized in Sec. 2.3.5.

3.1 PES inference for ground state

At first, the $(\omega_0, \omega_1) = (1, 0)$ case is performed to check the validity of our implementation. The depth D of the PQC, $U(\vec{\theta})$ or $U(\vec{\Theta})$, is varied from 2 to 6. Hence, the total number of parameters can be $2nD = 16 \sim 48$. The optimal parameters $(\vec{\theta}^*, \vec{\Theta}^*)$ for each depth model are summarized in appendix A. Once the optimal parameters $\vec{\Theta}^*$ are determined, the ground state energies at any bond length $b_{\text{test}} = \{b_l\}$ are inferred as follows,

$$E_0(b_l) = \langle \psi_0(b_l) | U^\dagger(\vec{\Theta}^*) \mathcal{H}(b_l) U(\vec{\Theta}^*) | \psi_0(b_l) \rangle, \quad (12)$$

where $|\psi_0(b_l)\rangle = G(\{\pi\langle\sigma_{z,l}^i\rangle\})|\phi_0\rangle$ as shown in the equation (8).

Figure 3(a) shows the results of PES inference of the ground state and full configuration interaction (FCI) calculation. One can clearly see the results of $D \geq 4$ match well the exact solution of the FCI method. Figure 3(b) shows the relative errors between each HQCNN model and the FCI method. The error in the case of $D = 6$ does not exceed the chemical accuracy, $\sim 1.6 \cdot 10^{-3}$ hartree. Hence, $D = 6$ is considered to have enough expressibility to describe the H_2 system.

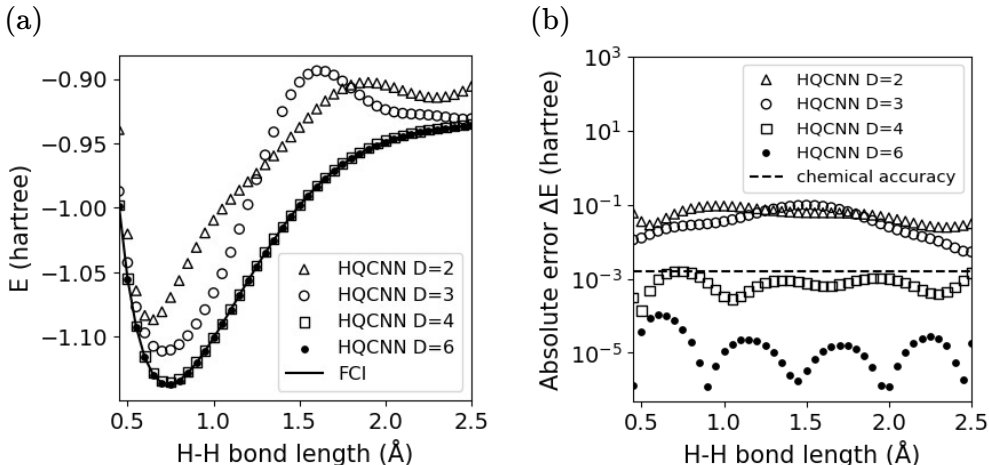


Figure 3: (a) PES inference for H_2 molecule using the $(\omega_0, \omega_1) = (1, 0)$ HQCNN model with each depth D . The solid line in the figure is drawn by full configuration interaction (FCI) calculation. (b) Absolute errors of the energies between each HQCNN model and FCI. The dotted line in the figure is drawn from the value of chemical accuracy, 0.001593 hartree.

To confirm consistency with Xia’s work [32], we have also calculated the PES without intermediate measurements, where full linear operation is performed by removing the classical layer. These results are summarized in Appendix B. From our calculation, the absence of a classical layer make inference accuracy worse. This is consistent with Xia’s

work and one can see that nonlinear connections between linear unitary operations are essential for highly accurate PES inference over the whole range of the bond length.

3.2 PES inference for both ground and excited state

The $D = 6$ condition is expected to have enough expressibility for the H_2 system described in Sec. 3.1. Next, the results of the $(\omega_0, \omega_1) = (1, 0.5)$ model with $D = 6$ are shown here. In this case, the parameters of the PQC are optimized to minimize the cost function $L_\omega = \langle L_0 \rangle + 0.5 \langle L_1 \rangle$ from the equation (11). By using the equation (7) for optimal parameters $(\vec{\theta}^*, \vec{\Theta}^*)$, the ground state energies E_0 and the excited state energies E_1 at any bond length $b_{\text{test}} = \{b_l\}$ are inferred by

$$E_j(b_l) = \langle \psi_j(b_l) | U^\dagger(\vec{\Theta}^*) \mathcal{H}(b_l) U(\vec{\Theta}^*) | \psi_j(b_l) \rangle \quad (j = 0, 1), \quad (13)$$

where $|\psi_j(b_l)\rangle = G(\{\pi\langle\sigma_{z,l}^i\rangle\})|\phi_j\rangle$ for two reference states $\phi_0 = |0000\rangle$ and $\phi_1 = |0001\rangle$ (little-endian for qubit ordering is used here.). The optimal parameters $(\vec{\theta}^*, \vec{\Theta}^*)$ are summarized in Appendix C.

Figure 4(a) shows the PES results from E_0 and E_1 inferred by the HQCNN model. Compared with the FCI method, the results of both states match well. Figure 4(b) shows the relative errors between results using the HQCNN model and the FCI method. We find that the error satisfies the chemical accuracy in both states and the PES inference for the excited state is slightly more accurate.

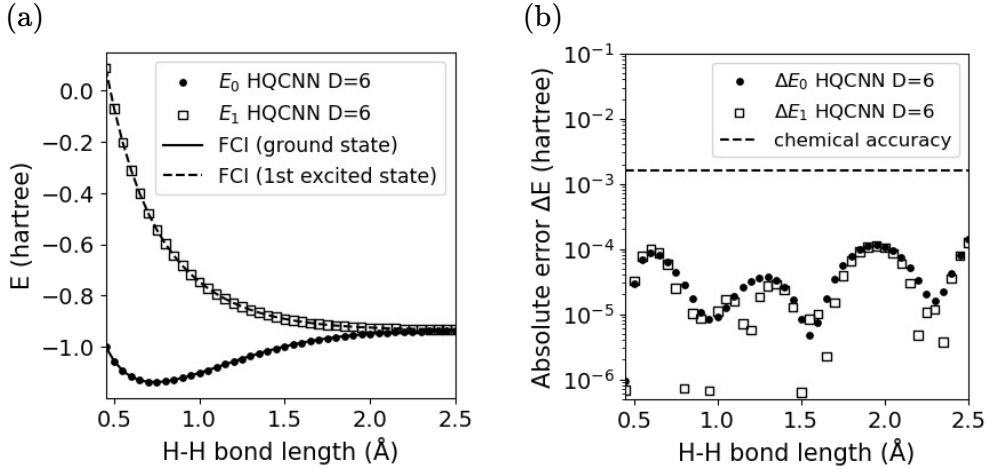


Figure 4: (a) PES inference of H_2 molecule using the $(\omega_0, \omega_1) = (1, 0.5)$ HQCNN model with $D = 6$. The solid and dashed lines in the figure are drawn by full configuration interaction (FCI) calculation. (b) Absolute errors between HQCNN model with $D = 6$ and FCI for E_0 and E_1 . The dashed line in the figure is drawn from the value of chemical accuracy, 0.001593 hartree.

3.3 Effect of sampling noise on PES inference

The results discussed so far are obtained on the statevector simulator, i.e., without noise due to sampling. On actual quantum hardware, the statevector cannot be observed and the noise effect from measurements is unavoidable. Here, focusing on the sampling noise only, the noise effect on PES estimation is simply discussed as follows: the parameters $(\vec{\theta}^*, \vec{\Theta}^*)$ of the HQCNN model are predetermined on the statevector simulator, and then

the energy estimation is performed by using the optimized HQCNN model on IBM’s qasm simulator [44].

Figure 5 shows the influence of shot number on PES inference. In the panel of Fig. 5(a) and (c), the PESs are plotted in the case of 10^3 and 10^5 shots. In the panel of Fig. 5(b) and (d), the energy differences ΔE_0 and ΔE_1 between the HQCNN model and the FCI method are displayed for each shot condition. One can see clearly that the errors eventually decrease as the shot number increases.

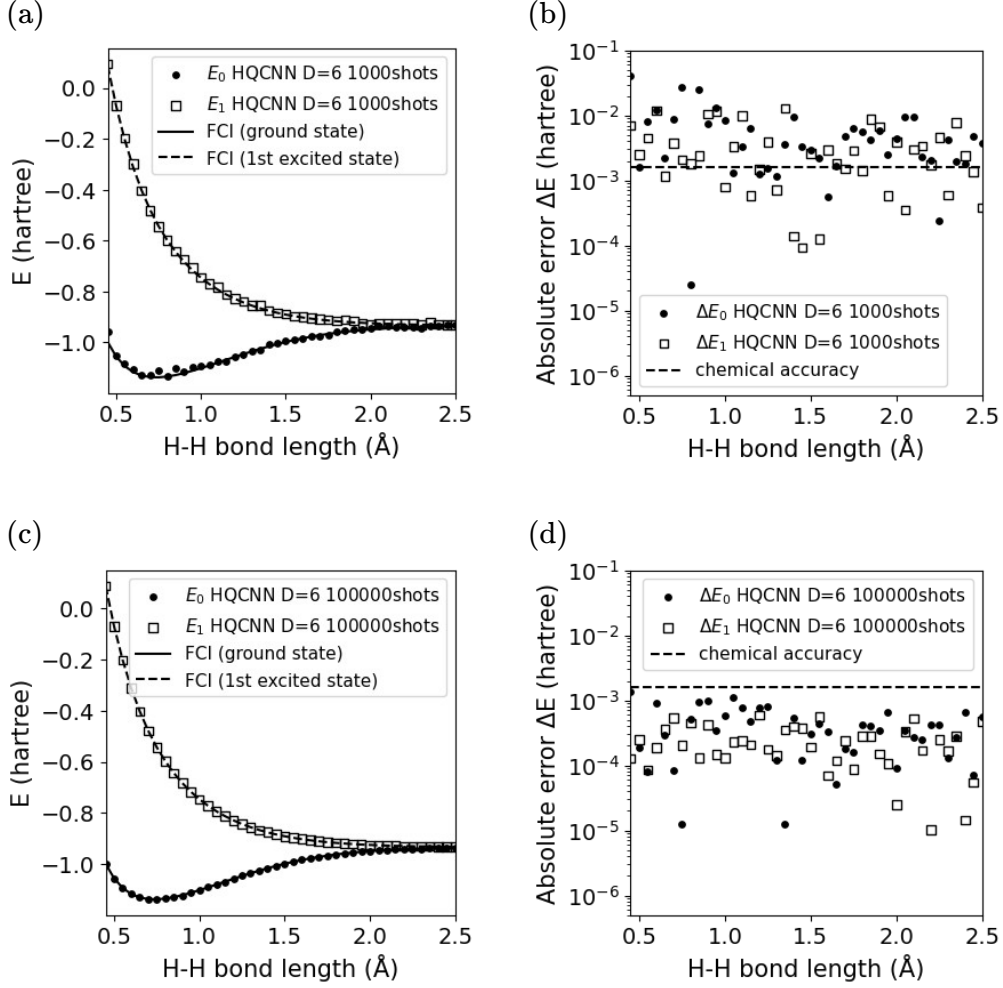


Figure 5: Sampling noise effects on PES inference of the $(\omega_0, \omega_1) = (1, 0.5)$ HQCNN model, where the expectation value of the energies are estimated on the qasm simulator. (a) PES of H₂ estimated by an HQCNN model with 1000 shots. (b) Absolute errors of the energies between the HQCNN model and FCI in the panel (a). (c) PES of H₂ estimated by an HQCNN model with 100000 shots. (d) Absolute errors of the energies between the HQCNN model and FCI in the panel (c). The dashed lines in the panel (b) and (d) are drawn from the value of chemical accuracy, 0.001593 hartree.

To evaluate quantitatively the sampling effect, a mean value and standard deviation (std) of ΔE_0 and ΔE_1 are also calculated. Figure 6 shows the mean and its std of ΔE_0 and ΔE_1 at each QASM shot condition. As a result, we find that inference performance improves as the QASM shots increase and at least $4 \cdot 10^4$ shots are required to satisfy the chemical accuracy.

As far as simulations with sampling noise are only concerned, our model can predict

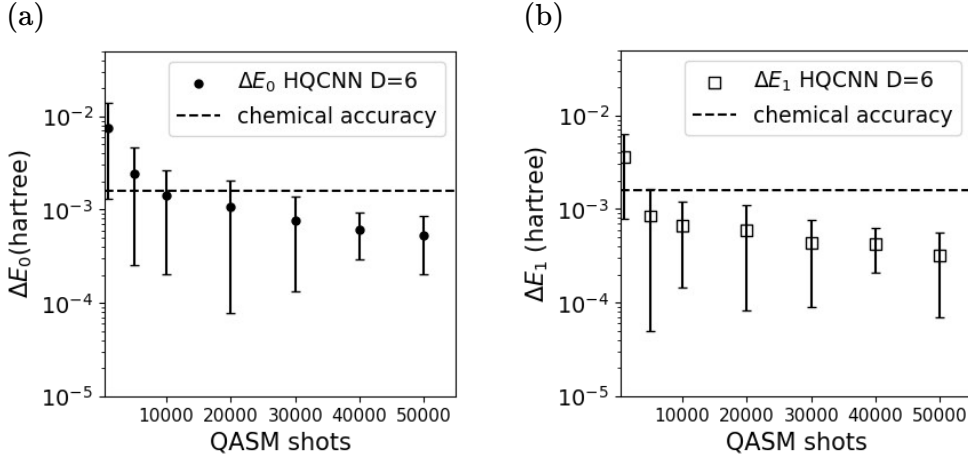


Figure 6: Absolute errors of PES between the HQCNN model and the FCI method at each QASM shot condition. Error bars in the figure represent standard deviation (std) from the mean. The dashed line in the figure is drawn from the value of chemical accuracy, 0.001593 hartree. (a) Mean and std of ΔE_0 at each shot condition. (b) Mean and std of ΔE_1 at each shot condition.

the energies of both ground and excited state with chemical accuracy when a sufficiently large shot number is set such as 10^5 . In our HQCNN model, the sampling noise for $\langle \sigma_z^i \rangle$ is also considered, therefore, the desired precision ε of the estimation could get worse, $\sim \varepsilon(1 + \sum_i \frac{\partial E_j}{\partial \langle \sigma_z^i \rangle} \frac{\langle \sigma_z^i \rangle}{E_j})$. According to the previous resource analysis [24], the total number of necessary measurements M can be estimated as $M = K/\varepsilon^2$, where K is a proportionality constant that depends on the Hamiltonian. In the case of H_2 molecule, K is about 0.1. Hence, $M > 4 \cdot 10^4$ shots is required for the chemical accuracy $\varepsilon \sim 1.6 \cdot 10^{-3}$. This is roughly consistent with the results in Fig. 6.

4 Discussion

Here we outline open perspectives. In this study, the PQCs that are part of the HQCNN model are optimized by using a noiseless statevector simulator. In principle, it can also be done on quantum hardware. However, the PQCs in this study are never a shallow circuit. As seen in the previous VQE study [47, 48, 49], a deep circuit based on hardware-efficient ansatzes causes troublesome phenomena, known as "barren plateaus" where gradients of a cost function vanish exponentially. Therefore, to train the HQCNN on quantum hardware efficiently, improving the PQC is essential. In addition, development of an efficient optimization method for minimizing the cost function [50] and an error mitigation technique are also important for efficient training of the HQCNN model and its highly accurate inference.

As another approach to estimate excited states, variational quantum deflation (VQD) [51] is well known. From the comparative study [52], VQD can exhibit better performance than SSVQE. Hence an HQCNN model where VQD is applied instead of SSVQE would enable more accurate prediction of energy. However, when VQD is applied to the HQCNN model, optimal PQCs for each excited state have to be prepared individually; in other words, the optimal parameter set $\vec{\Theta}_k$ for each excited state k must be determined through a training loop. On the other hand, in this SSVQE case, we just have to optimize one parameter set $\vec{\Theta}$ even if many excited states exist.

Finally, we refer to an encode layer to transform classical data to quantum data. This study focuses on a simple molecule, H_2 , because a simple encode gate, expressed in Eq. (3), is used. However, for a molecular configuration having more atoms, general encode layers will be needed. Following standard practices of quantum machine learning, ZZ feature map can be applied [11]. Further generalized encode layers are discussed in a recent study [53].

5 Conclusions

In summary, we have developed a hybrid quantum-classical neural network to predict the PESs of both the ground and the excited state with high accuracy. Our model is a surrogate model of the SSVQE in which mutually orthogonal initial states are prepared and a cost function for each state is calculated by combining PQC and measurements to achieve nonlinear operations. We have demonstrated that the proposed HQCNN can be trained for PES inference of the ground state and the 1st excited state for the H_2 molecule and the results can be obtained with chemical accuracy. Furthermore, we have presented the sampling noise effect on inference performance of the proposed model, and in view of that effect, a sufficiently large measurement such as 10^5 is ideally required for chemical accuracy. An interesting problem remains, namely, the question of how to improve PQC or the classical layer. This will be investigated in future work.

References

- [1] C. Cade, L. Mineh, A. Montanaro, and S. Stanisic, *Strategies for solving the Fermi-Hubbard model on near-term quantum computers*, Phys. Rev. B **102**, 235122 (2020).
- [2] A. Uvarov, J. D. Biamonte, and D. Yudin, *Variational quantum eigensolver for frustrated quantum systems*, Phys. Rev. B **102**, 075104 (2020).
- [3] W. J. Huggins, B. A. O’Gorman, N. C. Rubin, D. R. Reichman, R. Babbush and J. Lee, *Unbiasing fermionic quantum Monte Carlo with a quantum computer*, Nat. **603**, 416 (2022).
- [4] Y. Cao, J. Romero, J. P. Olson, M. Degroote, P. D. Johnson, M. Kieferová, I. D. Kivlichan, T. Menke, B. Peropadre, N. P. D. Sawaya, S. Sim, L. Veis, and A. Aspuru-Guzik, *Quantum Chemistry in the Age of Quantum Computing*, Chem. Rev. **119**, 10856 (2019).
- [5] S. McArdle, S. Endo, A. Aspuru-Guzik, S. C. Benjamin, and X. Yuan, *Quantum computational chemistry*, Rev. Mod. Phys. **92**, 015003 (2020).
- [6] B. Bauer, S. Bravyi, M. Motta, and G. K. Chan, *Quantum Algorithms for Quantum Chemistry and Quantum Materials Science*, Chem. Rev. **120**, 12685 (2020).
- [7] P. Rebentrost, M. Mohseni, and S. Lloyd, *Quantum Support Vector Machine for Big Data Classification*, Phys. Rev. Lett. **113**, 130503 (2014).
- [8] J. Biamonte, P. Wittek, N. Pancotti, P. Rebentrost, N. Wiebe and S. Lloyd, *Quantum machine learning*, Nat. **549**, 195 (2017).
- [9] H. Huang, M. Broughton, M. Mohseni, R. Babbush, S. Boixo, H. Neven and J. R. McClean, *Power of data in quantum machine learning*, Nat. Comm. **12**, 2631 (2021).
- [10] K. Mitarai, M. Negoro, M. Kitagawa, and K. Fujii, *Quantum circuit learning*, Phys. Rev. A **98**, 032309 (2018).

- [11] V. Havlíček, and A. D. Córcoles, K. Temme, A. W. Harrow, A. Kandala, J. M. Chow and J. M. Gambetta, *Supervised learning with quantum-enhanced feature spaces*, Nature **567**, 209 (2019).
- [12] M. Sajjan, J. Li, R. Selvarajan, S. H. Sureshbabu, S. S. Kale, R. Gupta, V. Singh and S. Kais *Quantum machine learning for chemistry and physics*, Chem. Soc. Rev., **51**, 6475 (2022).
- [13] P. S. Emani, J. Warrell, A. Anticevic, S. Bekiranov, M. Gandal, M. J. McConnell, G. Sapiro, A. Aspuru-Guzik, J. T. Baker, M. Bastiani, J. D. Murray, S. N. Sotiropoulos, J. Taylor, G. Senthil, T. Lehner, M. B. Gerstein and A. W. Harrow, *Quantum computing at the frontiers of biological sciences*, Nat. Methods **18**, 701 (2021).
- [14] R. Orus, S. Mugel, and E. Lizaso, *Quantum computing for finance: Overview and prospects*, Rev. Phys. **4**, 100028 (2019).
- [15] V. E. Elfving, B. W. Broer, M. Webber, J. Gavartin, M. D. Halls, K. P. Lorton, and A. D. Bochevarov, *How will quantum computers provide an industrially relevant computational advantage in quantum chemistry?*, arXiv:2009.12472 (2020).
- [16] K. Dalton, C. K. Long, Y. S. Yordanov, C. G. Smith, C. H. W. Barnes, N. Mertig, and D. R. M. Arvidson-Shukur, *Variational quantum chemistry requires gate-error probabilities below the fault-tolerance threshold*, arXiv:2211.04505 (2022).
- [17] S. Kanno, S. Endo, T. Utsumi and T. Tada, *Resource estimation for Hamiltonian simulation in correlated electron materials*, Phys. Rev. A **106**, 012612 (2022).
- [18] N. Yoshioka, T. Okubo, Y. Suzuki, Y. Koizumi, and W. Mizukami, *Hunting for quantum-classical crossover in condensed matter problems*, arXiv:2210.14109 (2022).
- [19] J. Preskill, *Quantum Computing in the NISQ era and beyond*, Quantum **2**, 79 (2018).
- [20] A. Peruzzo, J. McClean, P. Shadbolt, M.-H. Yung, X.-Q. Zhou, P. J. Love, A. Aspuru-Guzik, and J. L. O’Brien, *A variational eigenvalue solver on a photonic quantum processor*, Nat. Comm. **5**, 4213 (2014).
- [21] J. R. McClean, J. Romero, R. Babbush, and A. Aspuru-Guzik, *The theory of variational hybrid quantum-classical algorithms*, New J. Phys. **18**, 23023 (2016).
- [22] E. Farhi, J. Goldstone, and S. Gutmann, *A Quantum Approximate Optimization Algorithm*, arXiv:1411.4028 (2014).
- [23] K. Bharti, A. Cervera-Lierta, T. H. Kyaw, T. Haug, S. Alperin-Lea, A. Anand, M. Degroote, H. Heimonen, J. S. Kottmann, T. Menke, W.-K. Mok, S. Sim, L.-C. Kwek, and A. Aspuru-Guzik, *Noisy intermediate-scale quantum algorithms*, Rev. Mod. Phys. **94**, 015004 (2022).
- [24] J. F. Gonthier, M. D. Radin, C. Buda, E. J. Doskocil, C. M. Abuan and J. Romero, *Measurements as a roadblock to near-term practical quantum advantage in chemistry: Resource analysis*, Phys. Rev. Research **4**, 033154 (2022).
- [25] A. Eddins, M. Motta, T. P. Gujarati, S. Bravyi, A. Mezzacapo, C. Hadfield, and S. Sheldon, *Doubling the Size of Quantum Simulators by Entanglement Forging*, PRX Quantum **3**, 010309 (2022).
- [26] A. Arrasmith, L. Cincio, R. D. Somma, P. J. Coles, *Operator Sampling for Shot-frugal Optimization in Variational Algorithms*, arXiv:2004.06252 (2020).
- [27] M. Kohda, R. Imai, K. Kanno, K. Mitarai, W. Mizukami, and Y. O. Nakagawa, *Quantum expectation-value estimation by computational basis sampling*, Phys. Rev. Research **4**, 033173 (2022).

- [28] S. Endo, Z. Cai, S. C. Benjamin, and X. Yuan, *Hybrid Quantum-Classical Algorithms and Quantum Error Mitigation*, J. Phys. Soc. Jpn **90**, 032001 (2021).
- [29] J. Stokes, J. Izaac, N. Killoran and G. Carleo, *Quantum natural gradient*, Quantum **4**, 269 (2020).
- [30] J. Gacon, C. Zoufal, G. Carleo, and S. Woerner, *Simultaneous perturbation stochastic approximation of the quantum fisher information*, Quantum **5**, 567 (2021).
- [31] K. Mitarai, T. Yan, and K. Fujii, *Generalization of the Output of a Variational Quantum Eigensolver by Parameter Interpolation with a Low-depth Ansatz*, Phys. Rev. Applied **11**, 044087 (2019).
- [32] R. Xia, and S. Kais, *Hybrid Quantum-Classical Neural Network for Calculating Ground State Energies of Molecules*, Entropy **22**, 828 (2020).
- [33] A. Cervera-Lierta, and J. S. Kottmann, and A. Aspuru-Guzik, *Meta-Variational Quantum Eigensolver: Learning Energy Profiles of Parameterized Hamiltonians for Quantum Simulation*, PRX Quantum **2**, 020329 (2021).
- [34] K. M. Nakanishi, K. Mitarai, and K. Fujii, *Subspace-search variational quantum eigensolver for excited states*, Phys. Rev. Research **1**, 033062 (2019).
- [35] A. Aspuru-Guzik, A. D. Dutoi, P. J. Love and M. Head-Gordon, *Simulated quantum computation of molecular energies*, Science **309**, 1704 (2005).
- [36] P. Jordan and E. Wigner, *Über das Paulische Äquivalenzverbot*, Z. Phys. **47**, 631 (1928).
- [37] J. T. Seeley, M. J. Richard and P. J. Love, *The Bravyi–Kitaev transformation for quantum computation of electronic structure*, J. Chem. Phys. **137**, 224109 (2012).
- [38] A. Tranter, S. Sofia, J. Seeley, M. Kaicher, J. McClean, R. Babbush, P. V. Coveney, F. Mintert, F. Wilhelm and P. J. Love, *The Bravyi–Kitaev transformation: properties and applications*, Int. J. Quantum Chem. **115**, 1431 (2015).
- [39] K. Setia and J. D. Whitfield, *Bravyi–Kitaev superfast simulation of electronic structure on a quantum computer*, J. Chem. Phys. **148**, 164104 (2018).
- [40] A. Kokalj, *XCrySDen—a new program for displaying crystalline structures and electron densities*, J. Mol. Graphics Modelling **17**, 176 (1999). Code available from <http://www.xcrysden.org/>.
- [41] S. Sim, P. D. Johnson and A. Aspuru-Guzik, *Expressibility and Entangling Capability of Parameterized Quantum Circuits for Hybrid Quantum-Classical Algorithms*, Adv. Quantum Technol. **2**, 1900070 (2019).
- [42] J. Nocedal and S. J. Wright, *Numerical Optimization*, Springer: New York, NY, USA, **10**, p.978 (2006).
- [43] P. Virtanen, et al., *SciPy 1.0: Fundamental Algorithms for Scientific Computing in Python*, Nat. Methods **17**, 261 (2020).
- [44] G. Aleksandrowicz, et al., *Qiskit: An Open-source Framework for Quantum Computing*, (2021).
- [45] Q. Sun, et al., *PySCF: The Python-Based Simulations of Chemistry Framework*, Wiley Interdiscip. Rev. Comput. Mol. Sci. **8**, e1340 (2018).
- [46] J. R. McClean, et al., *OpenFermion: The electronic structure package for quantum computers*, Quantum Sci. Technol. **5**, 034014 (2020).

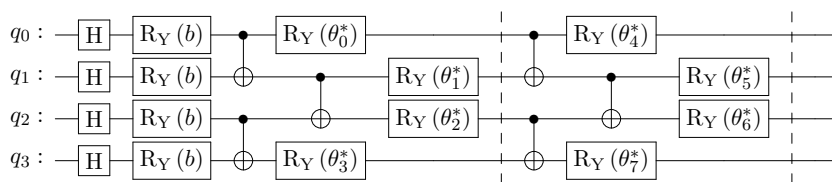
- [47] J. R. McClean, S. Boixo, V. Smelyanskiy, R. Babbush, and H. Neven, *Barren plateaus in quantum neural network training landscapes*, Nat. Commun. **9**, 4812 (2018).
- [48] S. Wang, E. Fontana, M. Cerezo, K. Sharma, A. Sone, L. Cincio and P. J. Coles, *Noise-induced barren plateaus in variational quantum algorithms*, Nat. Commun. **12**, 6961 (2021).
- [49] X. Liu, A. Angone, R. Shaydulin, I. Safro, Y. Alexeev and L. Cincio, *Layer VQE: A Variational Approach for Combinatorial Optimization on Noisy Quantum Computers*, IEEE Trans. Quantum Eng. **3**, 3100920 (2022).
- [50] M. Cerezo, A. Sone, T. Volkoff, L. Cincio and P. J. Coles, *Cost Function Dependent Barren Plateaus in Shallow Parametrized Quantum Circuits*, Nat. Commun. **12**, 1791 (2021).
- [51] O. Higgott, D. Wang, and S. Brierley, *Variational quantum computation of excited states*, Quantum **3**, 156 (2019).
- [52] Y. Ibe Y. O. Nakagawa, N. Earnest, T. Yamamoto, K. Mitarai, Q. Gao, and T. Kobayashi, *Calculating transition amplitudes by variational quantum deflation*, Phys. Rev. Research **4**, 013173 (2022).
- [53] O. Kiss, F. Tacchino, S. Vallecorsa and I. Tarverelli, *Quantum neural networks force field generation*, Mach. Learn.: Sci. Technol. **3** 035004 (2022).

A Optimal parameters of the $(\omega_0, \omega_1) = (1, 0)$ HQCNN model

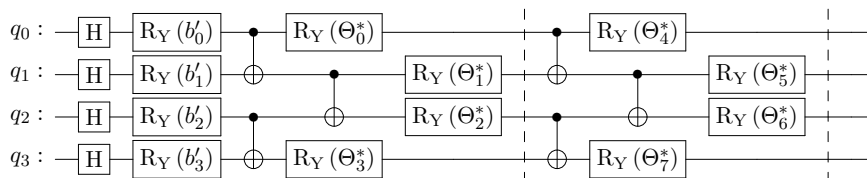
The optimal parameters $(\vec{\theta}^*, \vec{\Theta}^*)$ for the HQCNN model with each depth D are summarized as below. The parameterized quantum circuits defined in Eq. (4) and (5) are illustrated in Fig. 2. The optimal parameters $\vec{\theta}^* = \{\theta_0^*, \theta_1^* \dots \theta_{nD-1}^*\}$ and $\vec{\Theta}^* = \{\Theta_0^*, \Theta_1^* \dots \Theta_{nD-1}^*\}$ are fed into PQC1 and PQC2 respectively, as shown in Fig. 1.

A.1 D=2 for 4-qubits PQC

The quantum circuit combining PQC1 with Encode1 in Fig. 1 is illustrated as follows,



The quantum circuit combining PQC2 with Encode2 in Fig. 1 is illustrated as follows,



where, $\{b'_i\} = \{\pi \langle \sigma_z^i \rangle\}$. Then, the parameters $(\vec{\theta}^*, \vec{\Theta}^*)$ is summarized in the following table. The parameter-index i is incremented according to the order of the block circuit in Fig 2, i.e., the angle of R_y rotation gate on the i th qubit of D th block circuit is given by $\theta_{i+4(D-1)}^*$ for PQC1 ($\Theta_{i+4(D-1)}^*$ for PQC2).

i	θ_i^*	Θ_i^*
0	0.44990398	-0.07895043
1	0.00492587	-2.43631272
2	1.42098544	2.46370587
3	0.60825627	0.26725636
4	-0.47728727	-0.00459582
5	1.60923202	-1.55279297
6	0.38932374	-0.24098644
7	0.3966547	1.51973278

A.2 D=3 for 4-qubits PQC

i	θ_i^*	Θ_i^*
0	1.96276914e+00	-1.12944101e-03
1	1.25670686e+00	-5.46716619e-01
2	3.29694642e-01	8.29253916e-01
3	1.30778739e+00	1.16291385e-01
4	-8.11410342e-01	-2.53018795e-03
5	-2.13754993e-01	6.23986909e-03
6	2.40197722e-01	4.50162758e-01
7	1.41471586e+00	6.19085465e-02
8	7.42486302e-01	-9.55612005e-04
9	1.53853476e+00	5.00809978e-01
10	-1.01820297e-01	-8.19532007e-01
11	1.62537711e-01	1.58511488e+00

A.3 D=4 for 4-qubits PQC

i	θ_i^*	Θ_i^*
0	1.18244917	1.56155777
1	-0.03800419	-0.02127339
2	0.33551713	1.55263955
3	0.63058047	1.70198366
4	2.13454417	1.56133918
5	1.44831056	-0.00365438
6	1.03974931	0.00587906
7	0.08796629	0.02509409
8	2.08712489	-0.24766553
9	1.12208658	1.31541851
10	-0.52375853	2.20279135
11	0.77828267	-0.06444451
12	-0.97212089	-1.55945777
13	0.13481862	0.00841186
14	0.81579652	-0.00459007
15	0.42064851	1.51055261

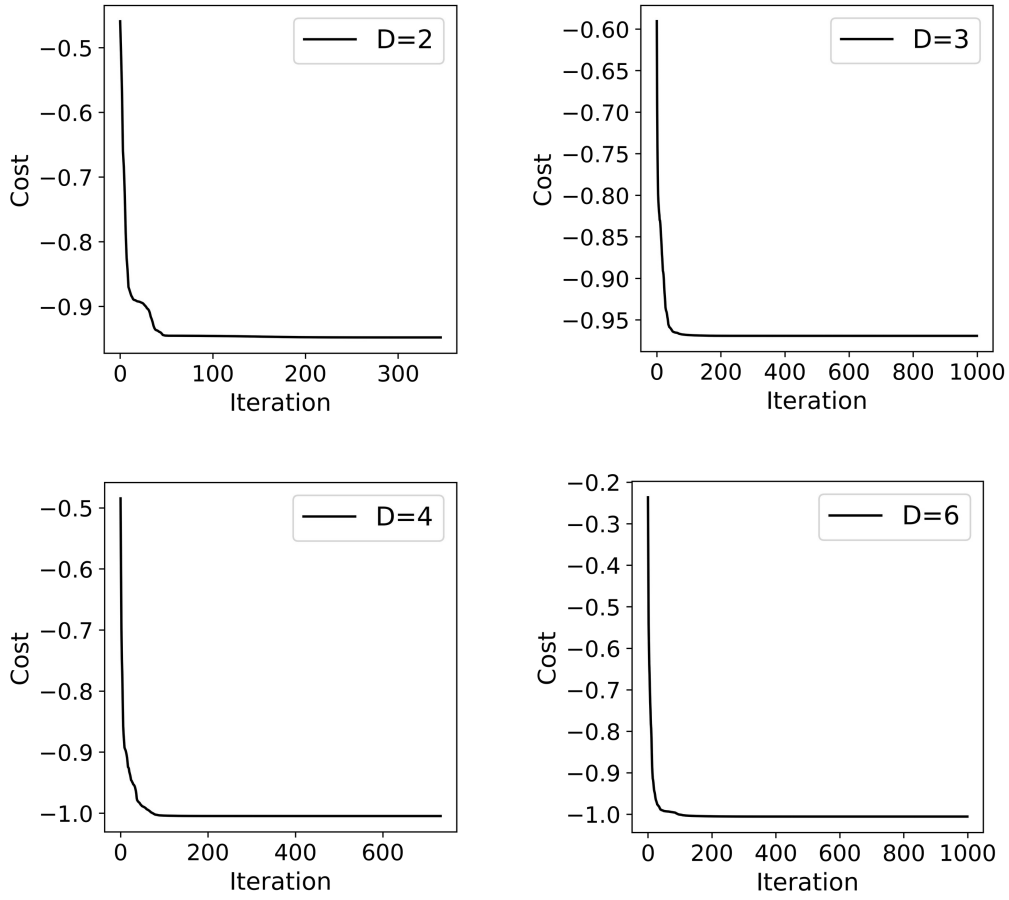


Figure A.1: Optimization process for each D case using BFGS optimizer. The computational conditions are summarized in Sec. 2.3.5

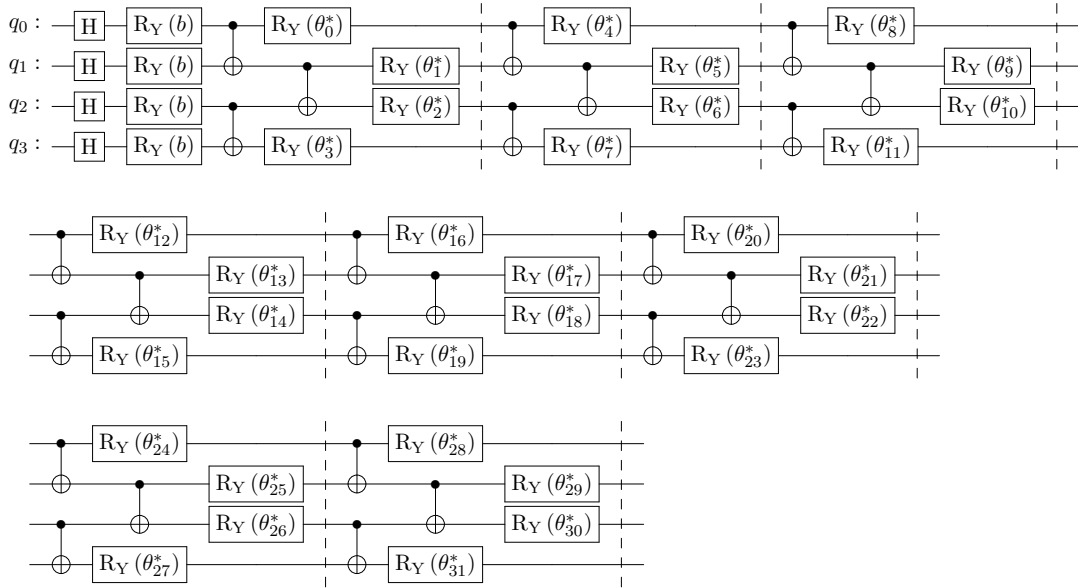
A.4 $D=6$ for 4-qubits PQC

i	θ_i^*	Θ_i^*
0	1.96944586e-01	2.16488379e-01
1	6.96085135e-01	-1.47369675e+00
2	2.75194632e-01	-6.09809058e-01
3	1.13995330e+00	2.18701015e+00
4	7.98447448e-01	4.54891917e-02
5	9.27048824e-02	-6.58927429e-02
6	1.39434016e+00	-3.64902005e-02
7	2.45081388e-01	-6.52573592e-01
8	5.50966511e-02	5.19154392e-04
9	-1.20161139e+00	3.60913707e-01
10	5.01887217e-01	-1.80183282e-01

11	4.12684265e-01	1.54652908e+00
12	1.05144072e+00	5.44473649e-04
13	1.87287163e-01	4.70659767e-01
14	-2.61354669e-01	-1.73169717e-01
15	6.14793737e-01	-1.11815028e+00
16	2.46727571e-01	4.58367070e-04
17	-4.15112509e-02	3.04351803e-01
18	3.09647969e-01	3.17354653e-01
19	1.68123352e+00	-3.38641312e-01
20	1.49119866e-01	-2.13794185e-03
21	1.90244017e-01	2.44324411e-01
22	1.47124686e+00	-2.27303510e+00
23	1.19942530e+00	2.22905860e-02

B Results with and without classical layer

The results of PES estimation with and without classical layer (C-layer) are displayed in Fig B.1. The parameterized quantum circuit without C-layer corresponds to the PQC1 with $D = 8$, in which the number of parameters $\{\theta^*\}$ is 32.



The optimal parameters θ_i^* are summarized as below.

i	θ_i^*
0	-2.21923412
1	1.75397721
2	-0.11685527
3	1.04819334

4 -0.60779518
 5 -0.03740226
 6 0.88396476
 7 0.44289291
 8 -0.04146204
 9 1.19623164
 10 0.49826975
 11 0.06755827
 12 -0.07466358
 13 0.61787473
 14 0.95700257
 15 -0.94629637
 16 1.46049613
 17 -0.3841755
 18 0.77517227
 19 1.31200736
 20 1.56461399
 21 1.43727198
 22 1.61064495
 23 2.16997706
 24 -0.05908558
 25 1.14194436
 26 -0.00621807
 27 0.79989797
 28 -0.58098377
 29 0.09029734
 30 0.0309237
 31 1.65240314

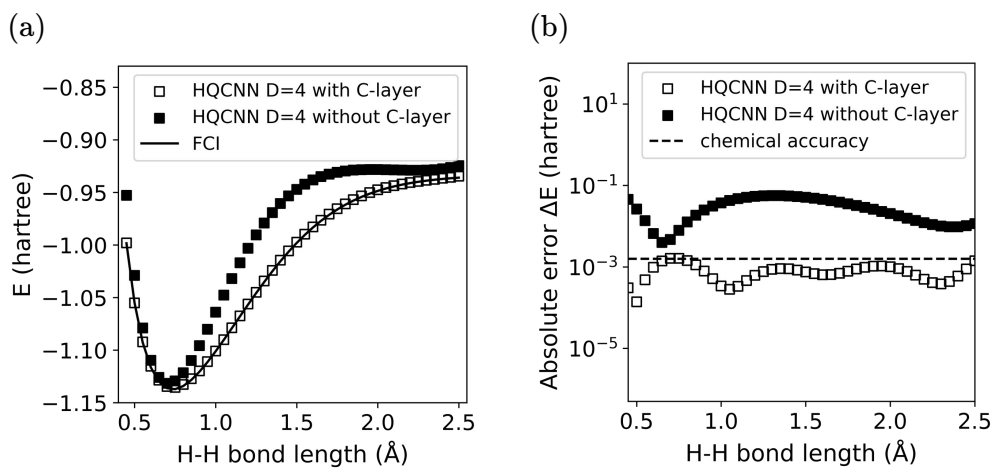


Figure B.1: (a) PES estimation for the H₂ molecule using the $D = 4$ HQCNN model with and without classical layer (C-layer) discussed in Sec. 3.3. (b) Absolute error of the energies between each HQCNN and the FCI method. The dotted line in the figure is drawn from the value of chemical accuracy, 0.001593 hartree.

C Optimal parameters of the $(\omega_0, \omega_1) = (1, 0.5)$ HQCNN model

C.1 $D=6$ for 4-qubits PQC

The optimal parameters $(\vec{\theta}^*, \vec{\Theta}^*)$ in Sec. 3.2 are summarized in the following table.

i	θ_i^*	Θ_i^*
0	4.06555514e-01	3.23397197e-01
1	3.90765681e-01	3.14126164e+00
2	1.28552322e-01	-5.20690613e-05
3	-2.03348271e-01	4.99569944e-01
4	8.52936329e-01	1.57060921e+00
5	1.09099632e+00	7.56231356e-05
6	-2.15279649e-02	-3.63973378e-04
7	3.19553075e-01	1.57068465e+00
8	5.42824781e-01	-8.81188684e-04
9	1.97727918e-01	1.44990590e+00
10	3.93177448e-01	9.48805894e-01
11	2.89423839e-01	-2.16437280e-04
12	4.57329007e-01	1.50413458e-04
13	-1.11312219e+00	1.57060129e+00
14	1.60299414e+00	-4.96648893e-01
15	9.58759382e-01	1.57073176e+00
16	-6.38281689e-01	1.57087092e+00
17	1.43562988e-01	1.57076878e+00
18	1.39205790e+00	6.21569280e-01
19	1.82419115e+00	-1.62844482e+00
20	4.95991802e-02	1.54094136e-05
21	6.24543518e-02	1.33004098e-05
22	-3.43793502e-01	1.57074102e+00
23	7.32904855e-01	1.17479292e-04

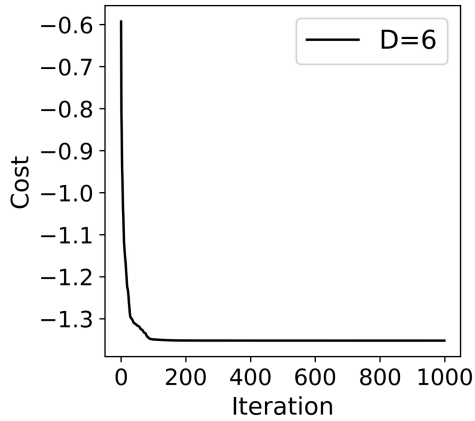


Figure C.1: Optimization process for $D = 6$ case using BFGS optimizer. The computational conditions are summarized in Sec. 2.3.5